Astron. Astrophys. 361, 321–326 (2000)

ASTRONOMY AND ASTROPHYSICS

Profiles of thermal line emission from advection dominated accretion flows

X. Cao[1,2]**, Y.D. Xu**[3]**, and J.H. You**[3]

[1] Chinese Academy of Sciences, Shanghai Astronomical Observatory, 80 Nandan Road, Shanghai, 200030, P.R. China
[2] Beijing Astrophysical Center (BAC), P.R. China
[3] Shanghai Jiaotong University, Department of Applied Physics, Shanghai, 200030, P.R. China

Received 26 January 2000 / Accepted 11 July 2000

Abstract. Recently, Narayan & Raymond (1999) proposed that the thermal emission lines from the hot plasma in advection dominated accretion flows (ADAFs) are potentially observable with the next generation of X-ray observatories, with which the physical properties of some X-ray sources can be probed. In ADAFs, the temperature of the ion is so high that the thermal broadening of the line is important. We calculate the profiles of thermal line emission from ADAFs, in which both the thermal and Doppler broadening have been considered. It is found that the double-peaked profiles are present for high inclination angles between the axis of disk and the line of sight. The double-peaked profiles are smeared in low inclination cases, and completely disappear when the inclination angle is less than 15°, where the thermal and turbulent broadening dominated on the line profiles. We also note that the thermal line profile is affected by the location of the transition radius of ADAF. The self-similar height-integrated disk structure and the emissivity with power-law dependence of radius are adopted in our calculations. The results obtained in this work can be used as a diagnosis on the future X-ray observations of the thermal lines. Some important physical quantities of ADAFs could be inferred from future thermal line observations.

Key words: accretion, accretion disks – line: profiles – X-rays: general

1. Introduction

Emission line profiles from accretion disks have been investigated by many researchers from both observational and theoretical sides. In the past decade, the X-ray line emission has been extensively studied, mainly stimulated by the progresses on X-ray observations. The profiles of emission lines from accretion disks around a Schwarzschild black hole (Fabian et al. 1989; Matt et al. 1993), or around a Kerr black hole (Laor 1991) are well calculated. The line spectra from ADAFs have been calculated by Fukue & Ohna (1997) without considering the thermal broadening of line profile in the rest frame of the emitter. The fluorescent line emission from cool gas irradiated by a hot corona, which is the focus in most X-ray line formation mechanism investigations, has been studied in some detail (Mushotzky et al. 1993; Tanaka et al. 1995). The fluorescent line can be formed in the disk region very close to the black hole. However, the thermal X-ray line emission from hot, optically thin gas around black holes has not been discussed very much. More recently, Narayan & Raymond (1999) presented the calculations on thermal line formation in hot ADAFs, and propose that such X-ray emission lines are potentially observable with the next generation of X-ray observatories. The physical properties of some X-ray sources and the constraints on the accretion flows in these sources may be provided by future observatories.

In a two-temperature ADAF, while the ions receive most of the viscous energy and are nearly virial, the electrons are heated by several processes, such as, Coulomb coupling with the ions, compression, and direct viscous heating, and cooled by a variety of radiation processes (Narayan & Yi 1995b). The temperature of the electron is in general lower than that of the ions due to insufficient interaction between electrons and ions(see Narayan et al. 1998 for a review on ADAFs). The thermal X-ray line emission is supposed to be from the disk region where the electron temperature is less than 10^9 K, which corresponds to the disk region $r > 100r_g$ (Narayan & Raymond 1999). The profiles of the fluorescent line are mainly determined by the Doppler broadening caused by the bulk motion of the flows, and thermal broadening can be neglected in the profile calculations. Unlike the case of the fluorescent line, the thermal X-ray lines are supposed to be from the disk region $r > 100r_g$ with the ion temperature around 10^{10} K. In this case, the thermal broadening of the line profiles is important compared with the Doppler broadening, since the bulk velocity of the ADAFs is only a fraction of the Kepler velocity, and the Kepler velocity at $100r_g$ is only one-fifth of that at the inner edge of the disk around a Schwarzschild black hole. In this work, we present calculations on the thermal line profiles from ADAFs. In Sects. 2-4, we give the formalism of the problem. The last section contains the results and a discussion.

Send offprint requests to: Xinwu Cao (cxw@center.shao.ac.cn)

2. Thermal broadening of the line profiles

We first calculate the thermal broadening of line emission from relativistic ions. Using the common relativistic transformations and assuming the motion of thermal ions to be isotropic, we write the observed flux density of the line from the ions moving at $\beta_i = v_i/c$ as

$$I_\nu(\gamma_i,\ \nu) = \frac{\epsilon_{\rm line}}{2\beta_i\gamma_i^3(1-\beta_i\mu)^2\nu_e}, \tag{1}$$

where $\epsilon_{\rm line}$ is the line emission power in the rest frame of the ion, ν, ν_e are the frequency measured by the observer and the line frequency measured in the emitter's frame respectively, γ_i is the Lorentz factor of the ion's thermal motion, and $\mu = \cos\theta$ (θ is the angle between the motion of the ion and the line of sight). Using the relation $\nu_e = \nu\gamma_i(1-\beta_i\mu)$, we can rewrite Eq. (1) as

$$I_\nu(\gamma_i,\ \nu) = \frac{\epsilon_{\rm line}\nu^2}{2\beta_i\gamma_i\nu_e^3}, \tag{2}$$

where

$$\frac{\nu_e}{\gamma_i(1+\beta_i)} \le \nu \le \frac{\nu_e}{\gamma_i(1-\beta_i)}.$$

If we consider an isotropic Maxwelliam distribution of the ions, the number density per unit energy is

$$N(\gamma_i) = \frac{1}{\Theta_{\rm ion}K_2(1/\Theta_{\rm ion})}\gamma_i(\gamma_i^2-1)^{\frac{1}{2}}e^{-\gamma_i/\Theta_{\rm ion}}, \tag{3}$$

where $\Theta_{\rm ion}$ is the thermal temperature in units of ion rest mass, and K_2 is the second-order modified Bessel function. The ion distribution function is normalized as

$$\int_1^\infty N(\gamma_i)d\gamma_i = 1.$$

We can therefore obtain the broadening profile of the thermal line emission as

$$\begin{aligned} I_\nu(\Theta_{\rm ion},\ \nu) &= \int N(\gamma_i)d\gamma_i\frac{\epsilon_{\rm line}\nu^2}{2\beta_i\gamma_i\nu_e^3} \\ &= \frac{\epsilon_{\rm line}\nu^2}{2\Theta_{\rm ion}K_2(1/\Theta_{\rm ion})\nu_e^3}\int_{\gamma_{\rm min}}^\infty \gamma_i e^{-\gamma_i/\Theta_{\rm ion}}d\gamma_i, \end{aligned} \tag{4}$$

where

$$\gamma_{\rm min} = \frac{\nu}{2\nu_e}\left[\left(\frac{\nu_e}{\nu}\right)^2+1\right].$$

For the given ion temperature $\Theta_{\rm ion}$, we can integrate Eq. (4) and obtain the line profile:

$$\begin{aligned} I_\nu(\Theta_{\rm ion},\ \nu) &= \frac{\epsilon_{\rm line}\nu^2}{2K_2(1/\Theta_{\rm ion})\nu_e^3} \\ &\times\left\{\frac{\nu}{2\nu_e}\left[\left(\frac{\nu_e}{\nu}\right)^2+1\right]+\Theta_{\rm ion}\right\}\exp\left\{-\frac{\nu}{2\nu_e\Theta_{\rm ion}}\left[\left(\frac{\nu_e}{\nu}\right)^2+1\right]\right\}. \end{aligned} \tag{5}$$

Besides the thermal broadening, the turbulent velocity of eddies in ADAFs may also affect the line profile. We assume the turbulence to be isotropic and adopt a mean turbulent velocity $v_t = \beta_t c$. The thermal line profile can be calculated by

$$\begin{aligned} I_\nu(\gamma_t,\ \Theta_{\rm ion},\ \nu) &= \frac{\epsilon_{\rm line}\nu^2}{4\beta_t\gamma_t K_2(1/\Theta_{\rm ion})\nu_e^3} \\ &\times\int_{x_{\rm min}}^{x_{\rm max}}\left(\frac{1+x^2}{2x^2}+\frac{\Theta_{\rm ion}}{x}\right)\exp\left(-\frac{1+x^2}{2\Theta_{\rm ion}x}\right)dx, \end{aligned} \tag{6}$$

where

$$x_{\rm min} = \gamma_t(1-\beta_t)\frac{\nu}{\nu_e},$$

and

$$x_{\rm max} = \gamma_t(1+\beta_t)\frac{\nu}{\nu_e}.$$

3. Structure of self-similar ADAF

We consider the self-similar disk structure given by Narayan & Yi (1994). In this solution, the azimuthal rotational velocity v_ϕ and radial velocity v_r are given as a function of r as follows:

$$v_r(r) = -\frac{5+3\epsilon'}{3\alpha^2}g(\alpha,\epsilon')\alpha v_K(r) \tag{7}$$

$$v_\phi(r) = \left[\frac{2\epsilon'(5+2\epsilon')}{9\alpha^2}g(\alpha,\epsilon')\right]^{1/2}v_K(r) \tag{8}$$

where,

$$v_K(r) = \left(\frac{GM}{r}\right)^{1/2},$$

$$\epsilon' \equiv \frac{\epsilon}{f} = \frac{1}{f}\left(\frac{5/3-\gamma}{\gamma-1}\right),$$

$$g(\alpha,\ \epsilon') \equiv \left[1+\frac{18\alpha^2}{(5+2\epsilon')^2}\right]^{1/2}-1.$$

It is assumed that magnetic fields contribute a constant fraction $(1-\beta)$ of the total pressure in ADAFs. The appropriate relation between the ratio of the specific heats γ and β is given by Esin (1997): $\gamma = (8-3\beta)/(6-3\beta)$. The disk structure is then described by three parameters: the ratio of the magnetic pressure β, the viscosity α, and the fraction f of viscously dissipated energy which is advected.

For simplicity, we further assume that the emissivity j of the unit area of disk surface has a power-law dependence on radius r,

$$j(r) \propto r^{-b}. \tag{9}$$

The radial velocity v_r and azimuthal velocity v_ϕ of the flow given by Eqs. (7) and (8) will be used in the calculations of line profile.

4. Profiles of thermal lines from ADAFs

Assuming the line of sight to be inclined at an angle i to the disk axis, the angle δ between the line of sight and the motion of gas in the disk is

$$\cos\delta = \sin i \cos\left(\phi + \theta_v + \frac{\pi}{2}\right), \tag{10}$$

where $\tan\theta_v = v_r/v_\phi$. Using the relativistic transformations, the line profile for a ring in the disk between r and $r+dr$ is available,

$$f_\nu(r,\ \nu_{\rm obs}) = rjdr\cos i \int \frac{I_\nu(\Theta_{\rm ion},\ \nu')}{\gamma_b^3(1-\beta_b\cos\delta)^3} d\phi, \tag{11}$$

where $\beta_b = \sqrt{v_r^2+v_\phi^2}/c$, $\gamma_b = \sqrt{1-\beta_b^2}$, and $\Theta_{\rm ion}$ is given by

$$T_i = 6.66\times10^{12}\frac{2(5+2\epsilon')}{9\alpha^2} g(\alpha,\epsilon')\beta r^{-1}. \tag{12}$$

The electron temperature T_e has been neglected in Eq. (12) (see Eq. (2.16) in Narayan & Yi 1995b), since T_e is about an order of magnitude lower than T_i in two-temperature ADAFs. In this paper, we focus our calculations mainly on iron, i.e., $\Theta_{\rm ion} = \frac{kT_i}{m_{Fe}c^2}$. The relation between ν' and $\nu_{\rm obs}$ is

$$\nu' = \nu_{\rm obs}\left(1-\frac{1}{r}\right)^{-1/2}\gamma_b(1-\beta_b\cos\delta) \tag{13}$$

where the factor $(1-1/r)^{-1/2}$ represents the gravitational redshift. From Eqs. (10) and (13), we can obtain

$$\frac{d\phi}{d\nu'} = \tag{14}$$
$$\frac{\left(1-\frac{1}{r}\right)^{1/2}}{\nu_{\rm obs}\gamma_b\beta_b\sin i\left\{1-\frac{1}{\beta_b^2\sin^2 i}\left[1-\frac{\nu'}{\gamma_b\nu_{\rm obs}}(1-\frac{1}{r})^{1/2}\right]^2\right\}^{1/2}},$$

Finally, we can calculate the line profile as

$$F_\nu(\nu_{\rm obs}) = \int_{r_{\rm in}}^{r_{\rm out}} rjdr\cos i \tag{15}$$
$$\times\int_{\nu'_{\rm min}}^{\nu'_{\rm max}} \frac{(\nu_{\rm obs}/\nu')^3\left(1-\frac{1}{r}\right)^{-1} I_\nu(\gamma_t,\ \Theta_{\rm ion},\ \nu')d\nu'}{\left\{\gamma_b^2\beta_b^2\nu_{\rm obs}^2\sin^2 i - \left[\gamma_b\nu_{\rm obs}-\nu'(1-\frac{1}{r})^{1/2}\right]^2\right\}^{1/2}},$$

where

$$\nu'_{\rm min} = \gamma_b\nu_{\rm obs}(1-\beta_b\sin i)\left(1-\frac{1}{r}\right)^{-1/2}$$

and

$$\nu'_{\rm min} = \gamma_b\nu_{\rm obs}(1+\beta_b\sin i)\left(1-\frac{1}{r}\right)^{-1/2}.$$

The inner and outer radii of the line emission region are assumed to be $r_{\rm in} = 100r_g$ and $r_{\rm out} = 1000r_g$. The typical turbulent velocity of eddies in ADAFs is approximated as $v_t \simeq \alpha c_s$, $c_s = \left(\frac{kT_i}{\mu_i m_u}\right)^{1/2}$, where $\mu_i = 1.23$ is adopted, same as Narayan & Yi (1995b). Now, using Eqs. (6) and (15), we can calculate the profiles of the thermal line from ADAFs.

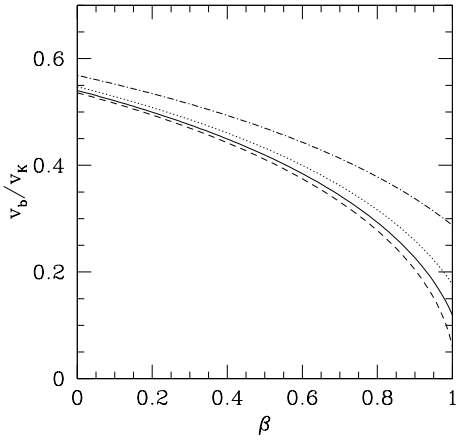

Fig. 1. The velocity of the accretion flow as functions of β for different values of viscosity: α =0.1 (dashed), 0.2(solid), 0.3(dotted), 0.5(dash-dotted), respectively.

5. Results and discussion

We show the total bulk velocity of the flow as functions of the disk parameters β and α in Fig. 1. It is found that the velocity is mainly determined by the value of β. The viscosity α affects the velocity very little, especially in the range of typical values of α around $0.2\sim0.3$ (Narayan et al. 1998). One may therefore draw the conclusion that the line profile is mainly determined by the value of the magnetic pressure ratio β that determines the ratio of specific heats γ here. We note that Quataert & Narayan (1999) give a different relation for the ratio of specific heats γ and plasma β, in which the particle heating is explicitly included. The plasma β is a function of the radius r, and the structure of ADAFs is therefore sensitive to the outer boundary condition. In this work we limit our calculations to Narayan & Yi's (1994) self-similar ADAF model in order to get the basic features of thermal line profiles. The present thermal line profile calculations can be easily extended for different ADAF models. The observed thermal line profiles would be used as tests on different ADAF models, and some physical quantities of ADAFs can be inferred from X-ray observations on thermal line profile and continuum emission.

In Figs. 2–4, we compare the importance of turbulent motions in the formation of the line profiles for different values of viscosity α. For small α, the turbulent velocity of eddies is small, and the line profiles are hardly affected by turbulence, while the profiles are obviously broadened in high α cases (see Fig. 4).

We adopt two sets of the disk parameters: A. $\alpha=0.2$, $f=1$, $\beta=0.5$; B. $\alpha=0.2$, $f=1$, $\beta=0.9$. The ratio of specific heats is $\gamma\simeq1.444$ for $\beta=0.5$, while $\gamma\simeq1.602$ for $\beta=0.9$. The line profiles for models A and B are plotted in Figs. 5 and 6, respectively. The exponent of the emissivity law is assumed to be $b=1$ in these calculations. We find that the double-peaked profiles appear at high inclination angles and are smeared by the thermal and turbulent broadening in low inclination cases. The double-peaked structure finally disappears when the line of sight is close to the axis of the disk. The bulk velocity of

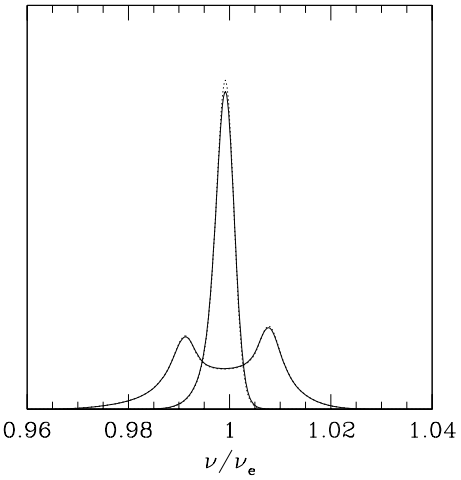

Fig. 2. The thermal iron line profiles with parameters: $\alpha = 0.1$, $\gamma = 1.444$ ($\beta = 0.5$), and $i = 0°$, $60°$, respectively. The dotted lines indicate the profiles without considering turbulent motions in ADAFs.

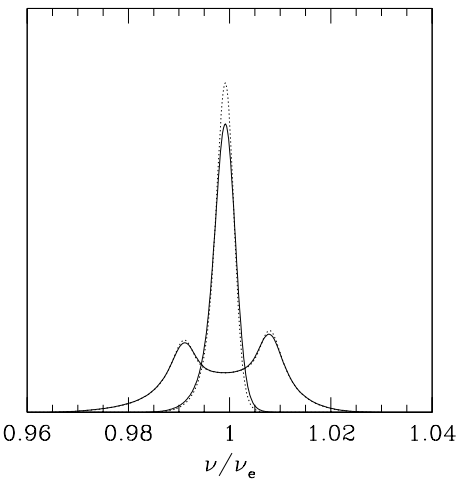

Fig. 3. Same as Fig. 2, but $\alpha = 0.2$.

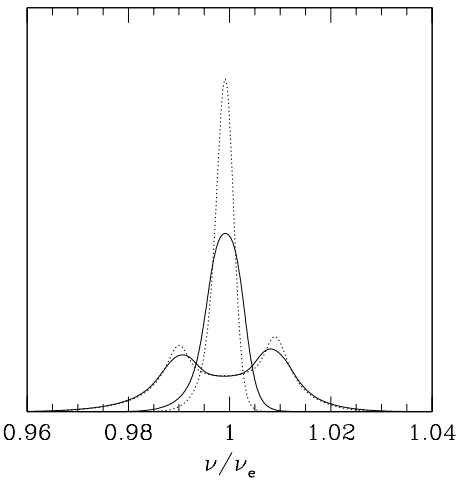

Fig. 4. Same as Fig. 2, but $\alpha = 0.5$.

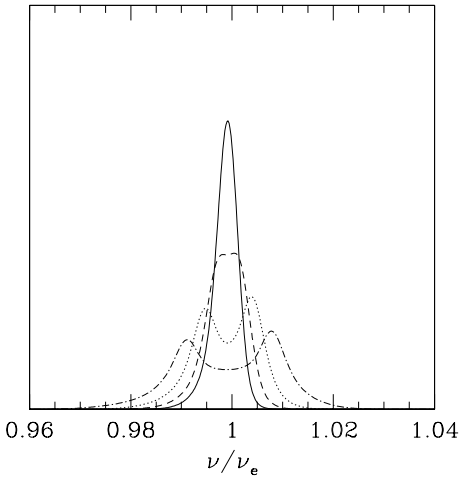

Fig. 5. The profiles of the thermal iron line emission from accretion flows for model A: $\alpha = 0.2$, $f = 1$, $\gamma = 1.444$ ($\beta = 0.5$), with different inclination angles: $i = 0°$(solid), $15°$(dashed), $30°$(dotted), $60°$(dash-dotted).

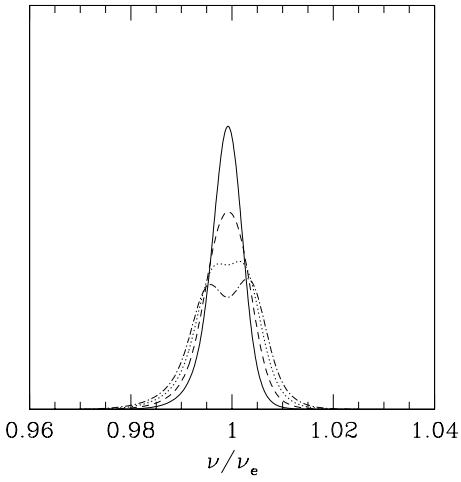

Fig. 6. The profiles of the thermal iron line emission from accretion flows for model B: $\alpha = 0.2$, $f = 1$, $\gamma = 1.602$ ($\beta = 0.9$), with different inclination angles: $i = 0°$(solid), $30°$(dashed), $45°$(dotted), $60°$(dash-dotted).

accretion flows is large in the low-β case, and one can then find in Figs. 5 and 6 that the wings of line profiles for model A extend over a larger range of frequency than that for model B. The double-peaked structure disappears completely when the inclination angle is about $15°$ for model A, while an obvious plateau is present at the inclined angle around $45°$ for model B (see Fig. 6).

In Figs. 7 and 8, the line profiles corresponding to the different emissivity law $b = 0,\ 1,\ 2$ are plotted for models A and B respectively. The line emission from the outer region of the disk dominates in the case of $b = 0$ and therefore has a narrower line profile, while a broader line profile is present in the case of $b = 2$, since the line emission is mainly from the inner region of the disk in this case where both the bulk and thermal velocities of the flow are high.

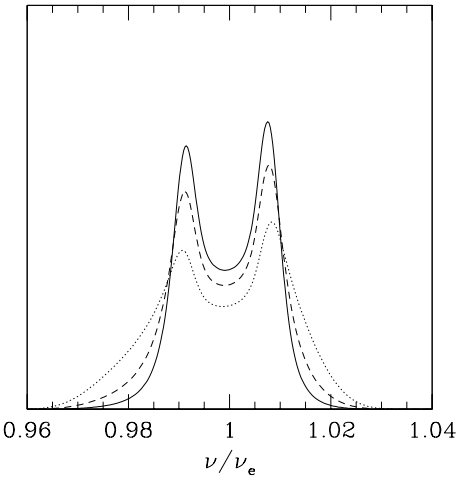

Fig. 7. The profiles of thermal iron line emission from accretion flows for model A with $i = 60^\circ$ for different emissivity law: $b =$ 0(solid), 1(dashed), 2(dotted).

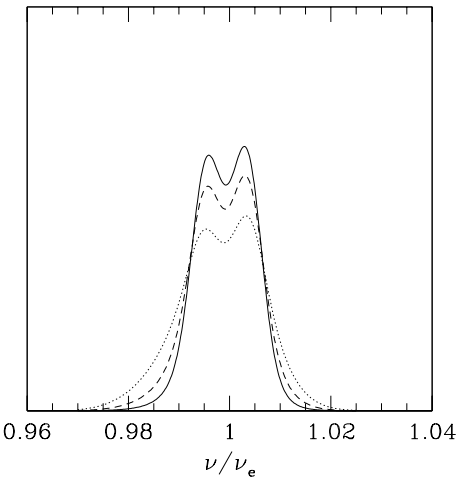

Fig. 8. Same as Fig. 7, but for model B.

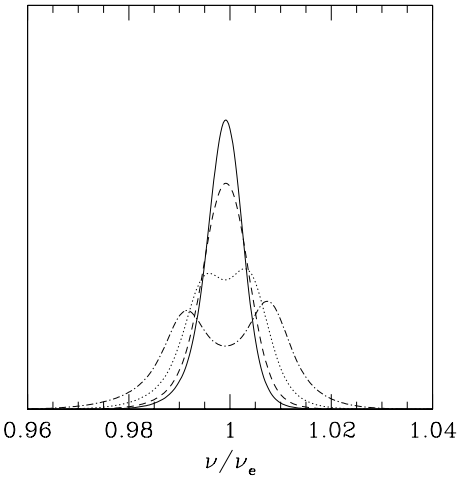

Fig. 9. Same as Fig. 5, but for thermal oxygen lines.

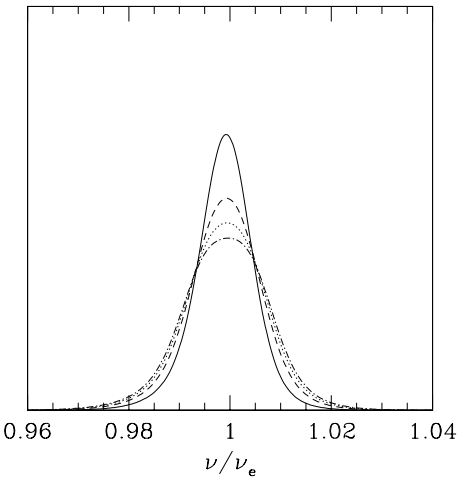

Fig. 10. The profiles of thermal oxygen line for model B, with different inclination angles: $i =$ 0°(solid), 45°(dashed), 60°(dotted), 75°(dash-dotted).

The line profile calculations in this work are mainly performed for iron, which would be most probably observed by X-ray observatories. We also plot the thermal oxygen line profiles in Figs. 9 and 10 for models A and B, respectively. It is found that the double-peaked structures are smeared even for high inclination cases. For model B ($\gamma = 1.602$), the bulk velocity of ADAF is relatively low, the double-peaked structure does not appear for any inclination angle, and only a plateau is present for the high inclination angle (see Fig. 10). The thermal lines for light ions have systematically broad profiles due to the fact that the lighter ion has higher thermal motion velocity for the same ion temperature. The expected difference between line profiles for different ions can be tested by future X-ray observations.

It is proposed that a transition radius r_{tr} exists in the ADAF model. In the region of $r < r_{tr}$, the accretion flow is a two-temperature ADAF, while in the region beyond the radius r_{tr}, the accretion occurs partially as a thin disk (Narayan et al. 1996). The profiles of thermal line will be obviously affected by the transition radius r_{tr}, which may be related to the accretion rate $\dot{m}$ (Narayan & Yi 1995b). In present line profile calculations, we have fixed the outer radius of line emission region as $1000r_g$. We depict the line profile dependence of the outer radius in Figs. 11 and 12. It is found that the line profile becomes narrow and a small difference between two peaks is present for a large outer radius. The outer region of the ADAF has relatively lower bulk velocity, and the emission from this region contributes mainly to the central part of the profile, which leads to a narrow line profile for a large outer radius. In the case of the ADAF with a small outer radius, the Doppler beaming effect caused by bulk motion of the flow in the whole line emission region is strong, and therefore the line profile is broad.

The line profiles are calculated on the assumption of the thermal distribution for ions (but also see Mahadevan & Quataert 1997). The thermal and turbulent broadening of the line is important, but the Doppler broadening by the motion of accretion flow cannot be neglected either. The profiles for thermal lines from ADAFs show that the blue peak is higher than the red

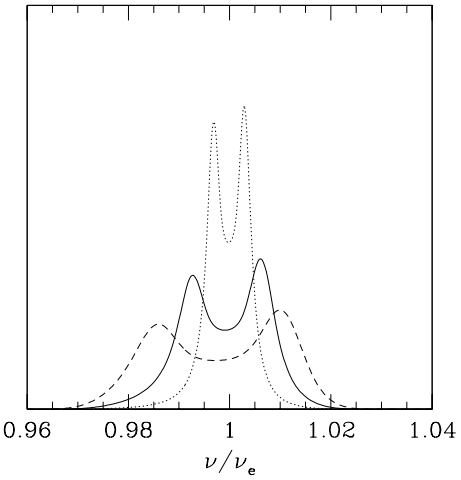

Fig. 11. The line profile dependence of the outer radius for model A: $r_{\rm out} = 300r_g$(dashed). $1000r_g$(solid), $5000r_g$(dotted). The inclination angle is $i = 45^\circ$.

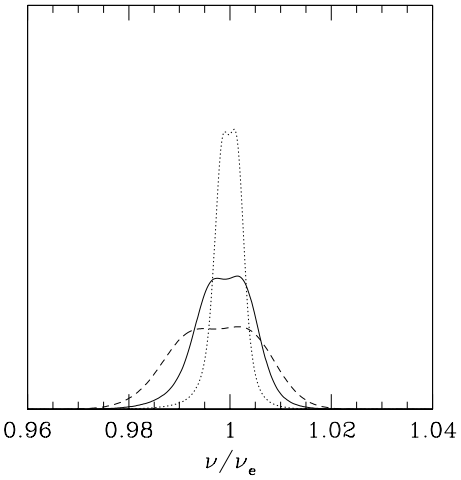

Fig. 12. Same as Fig. 11, but for model B.

one and line profiles extends more in the red wing, which is similar to previous calculations on the line profiles from the standard accretion disk. The difference between two peaks of the line from ADAFs is smaller than that of standard accretion disk cases, and the peaks are finally smeared by the thermal and turbulent broadening when the inclination is low. We note that the profiles of the neighbouring X-ray lines calculated by Narayan & Raymond (1999), for example, Fe XXVλ1.855 and Fe XXVIλ1.780, may partly overlap in high inclination cases. The present calculations on thermal line profiles can be used as a diagnosis on the future X-ray observations of the thermal lines.

We have not considered the Comptonization in ADAFs in present calculations, which may affect the thermal line profiles to some extent. It can be included in future line profile calculations, perhaps by numerical approaches (Dumont et al. 2000).

Our line profile calculations are based on the self-similar height-integrated ADAF models. The vertical structures of the velocity, density and ion temperature have not been taken into account. The velocity field in ADAFs may depend on the vertical height (Narayan & Yi 1995a; Igumenshchev & Abramowicz 1999). Narayan & Yi (1995a) studied the structure of ADAFs in the $r\theta$ plane by numerically solving the self-similar equations. They compared their exact self-similar solutions with those obtained using the system of height-integrated equations and found that various dynamical variables such as the radial velocity, angular velocity and sound speed estimated from height-integrated approximate solutions agree very well with the corresponding spherically averaged quantities in their exact solutions. Their exact solutions also show the angular velocity almost not varying with the angle θ at given radius r for small ϵ'. The present calculations can therefore be good approximations of the reality, provided the emissivity is interpreted as that from the shell at given radius r. We believe that the main features of line profiles have not been affected much by the limitation of one-dimensional velocity structure adopted in the calculations. Further calculations considering $r\theta$ distribution of variables v_r, v_ϕ, ρ and ion temperature T_i are necessary for detailed modelling of line profiles.

Acknowledgements. We acknowledge the referee's helpful comments. XC acknowledges Suzy Collin and Xuebing Wu for helpful discussion. This work is supported by the NSFC (No. 19703002), the Major State Basic Research Development Project, and Pandeng Project.

References

Dumont A.-M., Abrassart A., Collin S., 2000, A&A 357, 823
Esin A.A., 1997, ApJ 482, 400
Fabian A.C., Rees M.J., Stella L., White N.E., 1989, MNRAS 238, 729
Fukue J., Ohna E., 1997, PASJ 49, 315
Igumenshchev I., Abramowicz M., 1999, MNRAS 303, 309
Laor A., 1991, ApJ 376, 90
Mahadevan R., Quataert E., 1997, ApJ 490, 605
Matt G., Perola G.C., Stella L., 1993, A&A 267, 643
Mushotzky R.F., Done C., Pounds K.A., 1993, ARA&A 31, 717
Narayan R., Mahadevan R., Quataert E., 1998, In: Abramowicz M.A., Bjornsson G., Pringle J.E. (eds.) Theory of black hole accretion disks. Cambridge University Press, p. 148
Narayan R., McClintock J.E., Yi I., 1996, ApJ 457, 821
Narayan R., Raymond J., 1999, ApJ 515, L69
Narayan R., Yi I., 1994, ApJ 428, L13
Narayan R., Yi I., 1995a, ApJ 444, 231
Narayan R., Yi I., 1995b, ApJ 452, 710
Quataert E., Narayan R., 1999, ApJ 516, 399
Tanaka Y., Nandra K., Fabian A.C., et al., 1995, Nat 375, 659